ELSEVIER

Inversions of SIR-C and AIRSAR Data for the Roughness of Geological Surfaces

Robin Weeks, Milton Smith,* Kyung Pak,* and Alan Gillespie**

The surface roughness of alluvial fans in Death Valley, California, changes as the fans age. Because radar backscatter is sensitive to surface roughness, it is possible to map relative surface age using Synthetic Aperture Radar (SAR) data. We have examined surface roughness estimates in Death Valley from Shuttle Imaging Radar-C SAR data with the use of a technique that we call foreground/background analysis (FBA), with the goal of establishing a robust inversion method that is extendible to a range of surfaces and conditions. In this method, a foreground entity (in this case roughness) is distinguished from complicating background factors (including the distribution of intermediate-scale slopes, vegetation, and dielectric constant). The inversion for roughness is nonunique even when constrained by the use of field measurements. When the range of possible solutions is examined, it is observed that they fall into a small number of domains, each with distinct characteristics that are probably associated with physical factors such as the scale of roughness. Solutions were compared with those determined from the semiempirical (SEM) and integral equation (IEM) models, and all solutions were evaluated with respect to field knowledge. The SEM and IEM solutions, and those obtained using FBA together with the field measurements, fall into a common domain of solutions that are susceptible to contamination by background effects and hence may not be extendible to other geographic locations. A domain of stable solutions that are more extendible does exist; however, this extendibility is achieved at the expense of reduced resolution of roughness levels. For Death Valley, we estimate that it is possible to resolve only four levels of roughness, which is far fewer than can be theoretically resolved with existing inversion algorithms. ©Elsevier Science Inc., 1997

*Geological Remote Sensing Laboratory, University of Washington, Seattle

Address correspondence to Dr. Robin Weeks, Geological Remote Sensing Laboratory, University of Washington, Seattle, WA 98195.

Received 12 March 1996; revised 19 June 1996.

INTRODUCTION

Roughness and dielectric constant of the land surface are important parameters to many scientific disciplines. In the geological and geomorphological study of surfaces, for example, surface roughness is related to physical process and to exposure history. One of the objectives of the analysis of Shuttle Imaging Radar C (SIR-C) Synthetic Aperture Radar (SAR) data over land surfaces is the retrieval of these physical parameters. A number of approaches to this problem have been advanced that use field roughness and dielectric measurements from a given locality or type of surface to validate or develop inversion methods (Dubois et al., 1995; Oh et al., 1992; Shi et al., 1996). These methods are successful within the particular locality or on the particular surface type. However, it has not been demonstrated that they can be extended beyond the geographic locality and surface type on which they were developed and tested. This is due in part to the complexity of natural surfaces and in part to the paucity of adequate field data.

Many aspects of natural surfaces alter the radar backscatter. These include the surface roughness, the amount and type of vegetation, and the surface porosity and moisture. Roughness itself is a complex characteristic of surfaces that is dependent on spatial scale. Roughness at scales near the radar wavelength (5 cm for C-band), and at all scales greater, affects the radar backscatter. Therefore, radar response to roughness can be complex and variable from location to location. In Death Valley, the surface topography at different scales is controlled by sand grains, cobbles, washes, fans, and mountains. It is useful to treat roughness differently at different scales. We define the intrinsic surface roughness as microtopography at or near the scale of the radar wavelength; intermediate-scale roughness is larger-scale topography that is beneath the resolution of typical Digital Terrain Models (DTMs); and topography itself is resolved at the DTM scale (commonly 10s of meters). The field measurement of intrinsic surface roughness is a

REMOTE SENS. ENVIRON. 59:383–396 (1997)

655 Avenue of the Americas, New York, NY 10010

0034-4257/97/$17.00
PII S0034-4257(96)00161-7

painstaking, time-consuming process and, in a given field area, many such measurements are needed to characterize the variability in surface microtopography. Intermediate-scale topography is best characterized by using stereographic aerial photographs taken at low altitude (Farr et al., 1991). One objective of theoretical and empirical inversions of SAR data has been to determine the intrinsic surface roughness for natural surfaces. The existence of roughness at greater spatial scales adds complexity to an already difficult problem.

Commonly, effects of large-scale topography on radar backscatter are accounted for by using readily available DTMs. However, it is not possible to account for intermediate-scale effects, because the necessary DTMs do not exist. The effect of topographic complexity on the radar backscatter will propagate into the results of inversions for intrinsic surface roughness. In Death Valley, intermediate-scale topographic features are primarily due to networks of washes descending across the fans.

This topographic complexity, together with additional competing effects on the observed SAR signal, implies that a data set of high dimensionality is required for a unique inversion for intrinsic roughness. However, the various channels of SIR-C data (frequency and polarization) are, in general, highly correlated. This suggests that the intrinsic dimensionality of the data is small—certainly smaller than the number of physical variables that potentially affect the signal. It has been estimated that five parameters are required to completely describe the intrinsic surface roughness alone (Goff, 1995). Additional parameters are needed to describe intermediate scales of roughness, dielectric variation, and vegetation effects. Thus, the solution for physical parameters from SAR data is indeterminate, and we expect an infinity of potential solutions. Additional information is necessary to restrict the range of possible solutions. This provides motivation for the use of all possible bands of SAR data and of other data sets, such as Landsat Thematic Mapper (TM), that may also relate to roughness (Weeks et al., 1996). Field experience and knowledge also are particularly important in this respect.

In this article we explore a method of analysis called foreground/background analysis (FBA) that approaches the inverse problem in an adaptive way (Smith et al., 1996; Weeks et al., 1996). In some ways, foreground/background analysis (FBA) is similar to investigative strategies such as constrained energy minimization (Harsanyi, 1993; Farrand and Harsanyi, 1996). The SAR signature caused by undesired factors, such as those mentioned earlier, is labeled as "background," and the signature caused by intrinsic roughness is labeled "foreground." The actual foreground/background separation is accomplished by applying finite impulse response (FIR) filters to the different channels of radar data. We optimize the FIR filter by constructing a solution space from the set of all possible filters and examining this space for filters that minimize the background effects or maximize the foreground/background contrast. The FIR filter can also be optimized by using field data and/or other aspects of field knowledge such as the spatial distribution and ordering (in terms of roughness) of surfaces. The latter solutions are comparable to existing empirical inversions for roughness (Dubois et al., 1995).

One of the additional advantages of FBA is that it can be applied to other types of multispectral data and, hence, it provides a common framework of analysis. We have already demonstrated (Smith et al., 1996; Weeks et al., 1996) that VNIR data from Death Valley can be used to retrieve surface roughness parameters with almost as much success as that achieved with the use of SAR data, but the sensitivity of the retrieval depends on different aspects of the roughness. Hence, there may be advantages in combining analyses of SAR and visible and near infrared (VNIR) data and increasing the inherent measurement dimensionality.

We compare and examine field and image data, using different types of solutions for surface roughness. Using our own empirical solution for roughness, as well as the semiempirical model (SEM) (Dubois et al., 1995) and integral equation model (IEM) (Shi et al., 1996), we find that nonuniqueness poses significant difficulties in Death Valley. We then use FBA to examine the range of possible linear FIR filter solutions to estimate roughness in Death Valley from various SIR-C and airborne (AIR)SAR images. Within this range, we find types of solution that are less susceptible to nonuniqueness problems but have less resolution of roughness.

DATA AND METHODS

Field Data

The field roughness measurements have been described in detail by Weeks et al. (1996). Briefly, these were made at two spatial scales, using a stereophotography technique from which microtopograhic profiles could be extracted (Farr et al., 1991). Close-range, ground-based photographs were used to characterize the millimeter-to-meter scale topography, and low-altitude aerial photographs were used for the meter-to-100-meter scale. Measurements were made at 13 sites on alluvial fans in Death Valley, 11 of which are included in this study (Table 1 and Fig. 1. With the use of many profiles from a given site, a power spectrum of the surface topography is estimated. It is found that these power spectra conform closely to a power law. Because a power-law curve is a straight line in log-log space, it is possible to describe it by using two parameters that are characteristic of the individual surfaces: the slope and offset of the mean spectra in log-log space. The root mean square (rms) height of the surface is related to the area under the

Figure 1. TM image showing site locations of roughness measurements in Death Valley, California. At each site, the microtopographic profiles have been measured, using a close-up photogrammetric technique. Low-altitude photogrammetry at these sites has extended the scale of topographic measurements to 10s of meters.

power spectra, so greater offsets and lower slopes lead to higher rms heights. We determined these coefficients plus the rms height of the surfaces at the scale of the measurement from the measured profiles (Table 1).

Image Data

In this article, we analyze two calibrated, fully polarimetric SIR-C images of the Stovepipe Wells area in Death Valley (DT 35.01, DT 120.30) and an AIRSAR image (CM 3588). The SIR-C images were chosen to be from ascending and descending orbits, respectively, and to have similar look angles (Table 2). All image data were corrected to ground range and then registered to DT 35.01 to an accuracy of less than two pixels. Because the slopes of all the alluvial fan surfaces in the present study are less than 4°, we have not applied a terrain correction

Table 1. Results from Field Measurements of Surface Roughness at the Millimeter-to-Meter Scale Made by Using Close-Up Stereophotography at 11 Sites in Death Valley

Site	*Offset*	*Slope*	*RMS Height (cm)*
kfr	−1.88	−2.37	0.51
gt	−1.86	−2.45	0.58
kf3	−1.77	−2.50	0.68
gcl	−1.71	−2.62	1.15
kfw	−1.69	−2.41	0.91
kfl	−1.64	−2.71	1.06
kf2	−1.59	−2.57	1.10
md	−1.58	−2.52	0.98
gco	−1.54	−2.29	1.18
gcw	−1.47	−2.44	1.05
tc	−1.33	−2.64	1.65

The offset and slope of the surface power spectrum are given as well as the root mean square (rms) height. Sites are identified in Figure 1. The Trail Canyon (tc) site is about 20 km south of Stovepipe Wells.

to the image data. Results of an IEM-based solution (Shi et al., 1996) for roughness were supplied in image form by J. C. Shi.

Variation in Backscatter with Roughness

Figure 2 illustrates the relations between field data and measured backscatter for DT 35.01. For convenience, we have displayed relations only for C_{HH} and L_{HH} returns because these appear to be representative. Comparing the image data and field data, we find that the backscatter (σ°) averaged over a 5×5 pixel area (about 60×60 m) from the SAR imagery in all SIR-C bands is linearly related to the surface power-spectrum offset determined from the field measurements (Figs. 2a and 2b) with a fair degree of correlation ($r_0^2 \approx 0.7$). On the other hand, there is little correlation between mean σ° and the spectrum slope (Figs. 2c and 2d) and only a weak correlation with rms height (L-band has better correlation than C-band) (Figs. 2e and 2f). The surface power-spectrum offset is the most significant of the three roughness parameters for radar backscatter in Death Valley. This confirms earlier results in the U.S. southwest (Evans et al., 1992; Farr, 1992). In addition, from Figure 2 it can be observed that the relation between backscatter and roughness parameters is well described by linear models and that little or no improvement in fit would be gained from the use of nonlinear models.

Foreground/Background Analysis (FBA)

Here we describe an adaptive method of inverse analysis in which image data are subjected to finite impulse response (FIR) filters during FBA (Smith et al., 1994; 1996). FIR filters are linear filters of the form

$$Y_n = \sum_{q=1}^{nb} w_q \sigma_q + K, \quad (1)$$

where Y_n is the output of the filter, σ is the input signal that consists of nb channels or bands, w is the filter, and K is a constant. In our case, the input signal is the SAR image data (σ_q consisting of as many as six bands of data per pixel) to which the filter weights (w_q) are to be applied to produce Y_n, the estimate of the desired quantity (intrinsic roughness). The filter, operating in the spectral domain (wavelength and polarization), is simply a linear transformation of the image bands. Because the relation between backscatter and roughness is dominantly linear in Death Valley (Fig. 2), the use of a linear approach is justified, at least provisionally.

FBA was developed as an extension of spectral mixture analysis (SMA) by separating the FIR filter into two sets of equations:

$$\text{Foreground: } Y_f = \sum_{q=1}^{nbands} w_q \sigma_q + K + \varepsilon, \text{ where } f = 1 \ldots n_f \quad (2)$$

$$\text{Background: } Y_b = \sum_{q=1}^{nbands} w_q \sigma_q + K + \varepsilon, \text{ where } b = 1 \ldots n_b \quad (3)$$

and where the w_q are again the weights of the filter for which we solve by using singular value decomposition (SVD) and n_f and n_b are the number of foreground and background spectra used in the analysis. As formulated in Eqs. (2) and (3), any number of spectra are used to identify w. Rather than unmixing the image spectra for the fractions of a set of known constituent spectra (as in SMA), FBA estimates the amount of a foreground quantity (in our case, intrinsic roughness) in the presence of a potentially complex (multiple spectra) background. The accuracy in the foreground quantity depends on the background complexity and, for a given background complexity, we can determine the potential error in foreground estimation.

In this article, we use the simple FIR filter approach only [Eq. (1)]. We have separated the FBA analysis into two types: one where the filter is used in the inverse

Table 2. Synthetic Aperture Radar Image Parameters for Data Used in This Study

ID	*Look Angle*	*Track Angle*	*Wavelengths*	*Pixel Spacing*	*Polarizations Used*
DT 35.01	46.6°	42.7°	*C,L*	13.3 × 4 m	HH,VV
DT 120.30	45.6°	141.6°	*C,L*	13.3 × 5.2 m	HH,VV
CM 3588	40.1°	162.4°	*C,L*	12.1 × 6.7 m	HH,VV

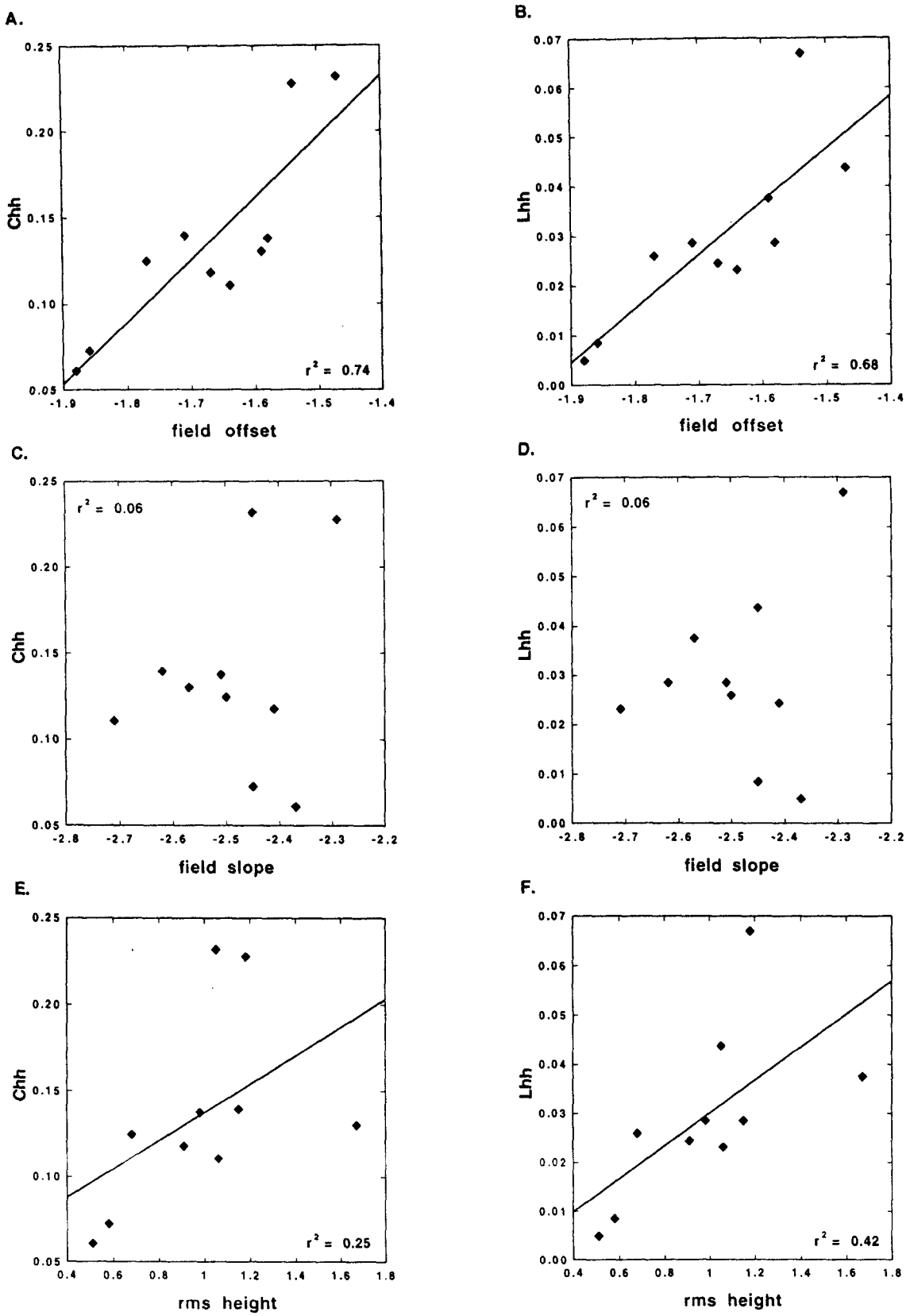

Figure 2. The relation between field data and average backscatter from the image data for DT 35.01. Where appropriate, linear best fits are displayed together with the value of r^2. (a) Variation in C_{HH} with surface power spectrum offset. (b) Variation in L_{HH} with surface power spectrum offset. (c) Variation in C_{HH} with surface power spectrum slope. (d) Variation in L_{HH} with surface power spectrum slope. (e) Variation in C_{HH} with surface rms height. (f) Variation in L_{HH} with surface rms height. Weak correlations with slope and rms height have been shown in other studies.

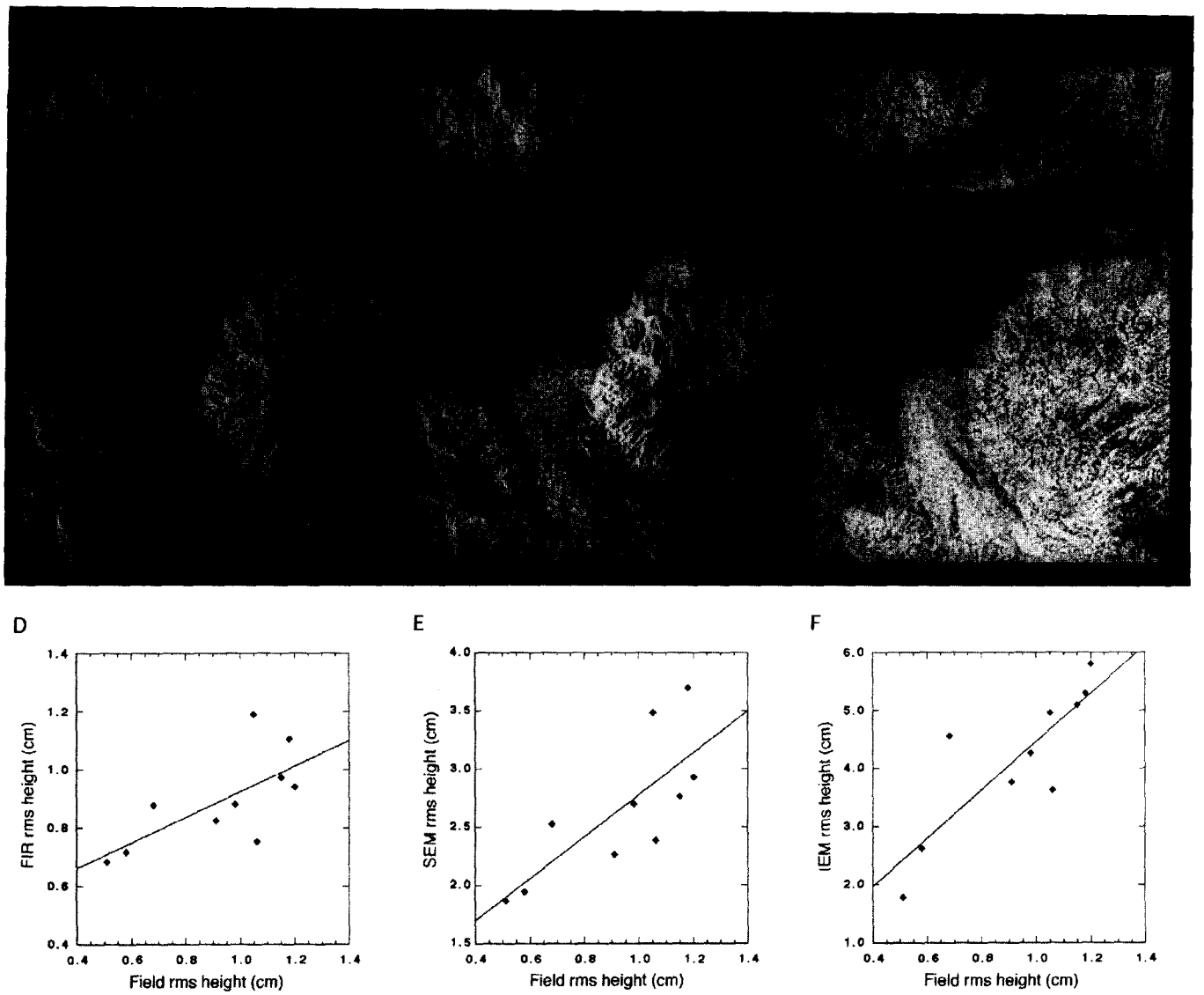

Figure 3. Results for DT 35.01 of three different inversions for surface rms height and a comparison with surface data: (A) the FIR model (optimized by using the field rms height data) (S, location of Stovepipe Wells); (B) the SEM solution (Dubois et al., 1995); (C) the IEM solution (Shi et al., 1996); (D) comparison of FBA results with field rms data; (E) comparison of SEM results with field rms data; (F) comparison of IEM results with field rms data. The scales on the y axes are different.

sense (empirical FBA) and the other where the filter is used in the forward sense (generalized FBA). These are fully described in the following sections. We present the empirical FBA method merely as a means of introducing the application of FIR filters to image data. Because empirical FBA uses field measurements to constrain the solution of the FIR filter, our solution is optimized for Death Valley, and we expect improved results compared with other methods, such as the SEM model (Dubois et al., 1995), which have not been optimized under these conditions. However, we also expect that the nature of the empirical FBA solution will be similar to the other algorithms in that it will not, for reasons to be discussed, be reliably extendible to other geographical regions and surface types. The generalized FBA technique was developed to produce extendible solutions, and, although the extendibility characteristic remains to be verified, the presentation of this approach is the main point of this article.

Empirical FBA

In this simplest application of FBA, the field roughness measurements are used to constrain the solution for the FIR filter. Spectra are extracted from the SAR images at the locations of the field sites. These spectra are input into a set of equations of the form of Eq. (1) where the Y's are the field measurements of roughness for the corresponding sites. With 11 sites, there will be 11 equations that are solved for the unknown w vector, using SVD. This w vector will be the optimum linear filter to retrieve the field measurements from the SAR spectral data for the sites under consideration. When obtained, this filter can then be applied to the entire image (see Fig. 3a).

There are a number of disadvantages with this type of solution. Unless the field measurements of roughness uniquely account for the image variability, these solutions will represent only a small subset of the range of possible solutions. Much depends on the accuracy and completeness of the field data in capturing all of the surface variability and, given the difficulty in making field measurements of roughness, it is unlikely that enough measurements will be available to constrain the solution reliably. The solution, though accurate at the location of the field sites, is free to deviate at all other locations. In addition, it may be possible to obtain good fits to the field data by using very different types of solutions (different w vectors). Hence, it is hard to estimate the degree to which solutions are contaminated by background factors.

Generalized FBA

A more complete analysis uses FBA to examine the performance of the solutions throughout a comprehensive range of filters. Instead of assuming (as above) *a priori* knowledge of the outputs (Y_n), we artificially generate the filters (w) to produce a range of outputs or solutions (Y). The intention is to analyze the entire possible range of solutions, which in this case is restricted for simplicity to all linear combinations of C- or L-band or both copolarized channels. To compare the many solutions, numerical characteristics from the resulting solution image of each filter are calculated. These numerical characteristics are called "objective functions." In this article, we define the objective functions by choosing subsets or regions of the solution image that are assumed to represent extremes of roughness encountered in Death Valley. The objective function for the foreground is defined as the difference between rough and smooth subsets, and the function for the background is defined as the mean variance within both subsets. For each of the solutions, Y, the foreground and background objective functions are calculated. As we cycle through all possible combinations of band weights (w_q), the values from the objective functions are plotted as solution surfaces—one for the foreground and another for the background. These surfaces characterize the solution space. The foreground surface represents a description of the solution space that quantifies the effectiveness with which the FIR filters detect roughness in the presence of clutter or background variability (as we have defined it). It is observed in the results section that there are distinctive regions on these surfaces where the influence of background factors is minimized.

RESULTS

Empirical FBA, SEM, and IEM Models

The theoretical and empirical inversions for intrinsic roughness in Death Valley are nonunique. We illustrate this problem, first, by examining the results of different inversion algorithms for a single SIR-C image, and then we examine the results for a sequence of ascending- and descending-pass images, using a single inversion method. Figure 3 shows results from SIR-C DT 35.01 for three different inversion models for rms height: the empirical foreground/background (FBA), the semiempirical (SEM), and integral equation (IEM). For the FBA solution (Fig. 3a), field-measured rms heights were used to constrain the solution. The SEM and IEM (Figs. 3b and 3c) have similar magnitudes and the same contrast stretch, and they are directly comparable to each other. However, the FIR model results are quite different in magnitude, and a different stretch has been necessary to display the result. All models show a gross similarity in the pattern of roughness differences; for example, they indicate that the lower east side of the valley is smoother than the west side. The models all produce a roughly linear fit to the field data for rms height (Figs. 3d–3f). However, in detail, there are differences in the ordering of surfaces, and, more strikingly, we find that the SEM and IEM overestimate the field measurements by a factor of two to five.

When we inspect the results, a second difficulty comes to light when we compare results of a single inversion algorithm for images with different look directions. Figure 4 illustrates SEM rms height solutions from two SIR-C data takes that have look directions approximately at right angles to one another. DT 35.01 is an ascending data take that looks primarily along the axis of Death Valley, and DT 120.3 is a descending data take whose look direction is roughly perpendicular to the main valley. The SEM solutions are markedly different, especially on the east side of the valley where the ascending pass produces solutions that have as much as 30% greater rms heights.

Generalized FBA

In generalized FBA, we examine the entire range of linear solutions. For comparison with the SEM and IEM algorithms, which use single-band, copolarized channels, we first develop the FBA approach separately on C- and L-band copolarized channels. The method is then extended to analyze C- and L-bands jointly. Figure 5 illustrates the solution profiles determined for C-band copolarized channels for both DT 35.01 and DT 120.30. The x axis is an angle from 0° to 180° that is used to generate the normalized band weights (w) for HH and VV bands, respectively; the sine of the angle becomes the weight for HH polarization and the cosine is the weight for VV; so any point along the axis represents a linear FIR filter that can be applied to the image data, and the entire axis includes all possible linear combinations of HH and VV polarizations. This arrangement is somewhat arbitrary and is merely designed to allow us to cycle through the range of possible combinations of HH and VV in a systematic way. The result of the objective is plotted on the

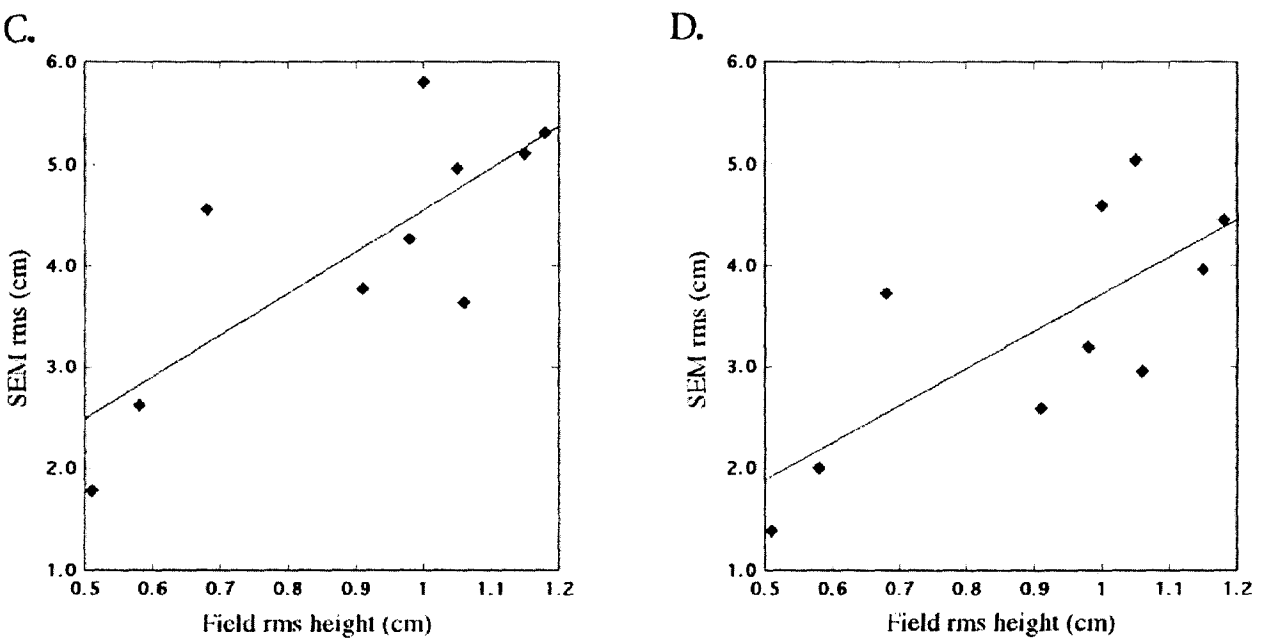

Figure 4. Results of the SEM inversion for rms height for two different SIR-C images: (A) DT 35.01 is an ascending-pass image (essentially perpendicular to the mean wash orientation); (B) DT 120.30 is a descending-pass image (parallel to the mean wash orientation); (C) and (D) show a comparison of the SEM results with the field rms height data for DT 35.01 and DT 120.30, respectively.

y axis; for the foreground plot (Fig. 5a), this is the difference between image subsets of contrasting roughness; for the background plot (Fig. 5b), it is the mean variance within both subsets. These subsets have been chosen by using field knowledge but could have been chosen by using recognized geological features, such as alluvial fans (rough) versus playa (smooth). By moving along the x axis and, hence, cycling through all possible w vectors

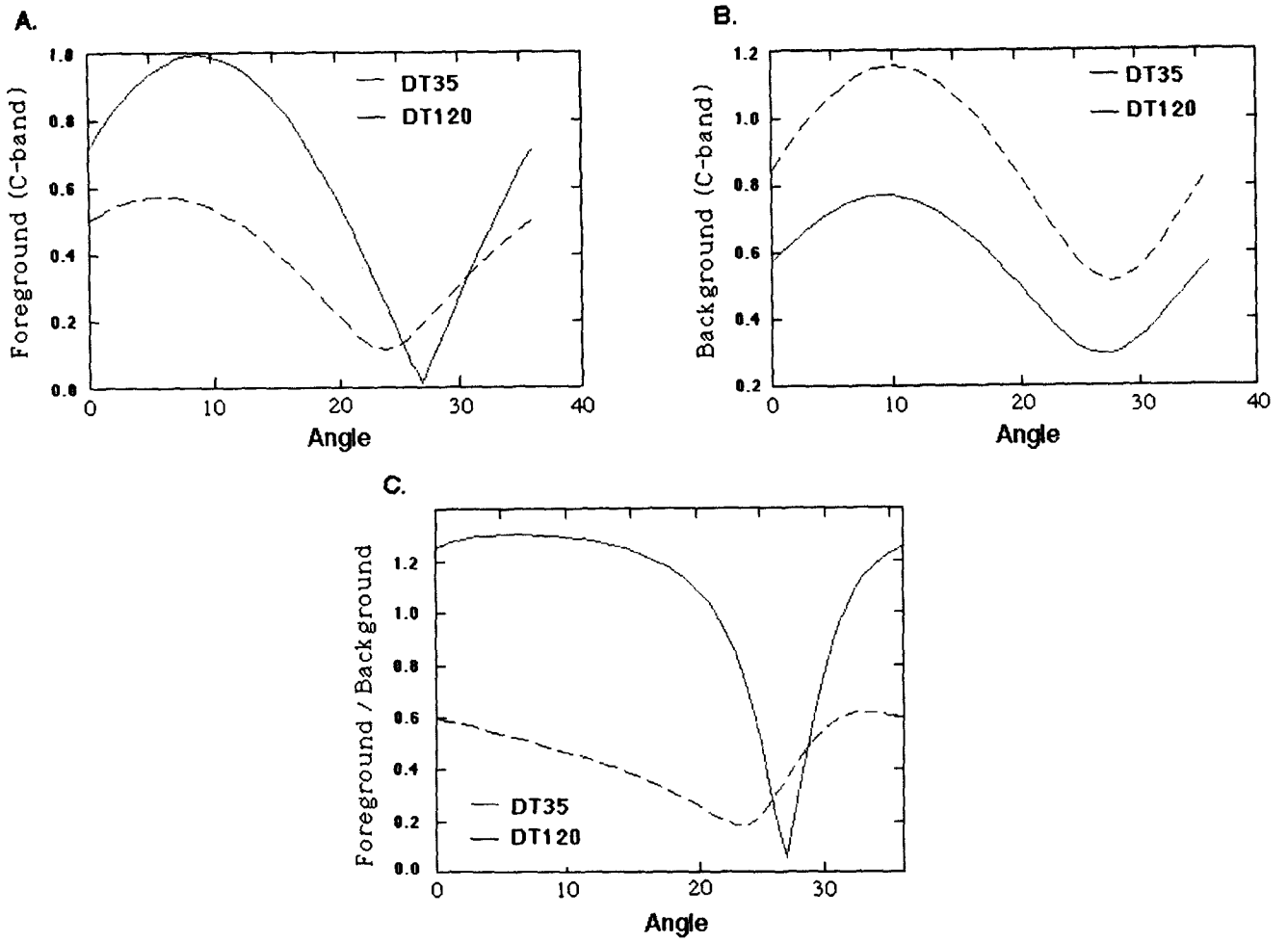

Figure 5. FIR solution profiles for rms height for C-band copolarized channels of DT 35.01 (dashed line) and DT 120.30 (solid line). The x axis is an angle used to generate FIR filter weights for HH and VV polarizations. The sine of the angle is w_{HH} and the cosine of the angle is w_{VV}. Each point on the x axis is, therefore, a separate FIR filter, and moving along the x axis is equivalent to cycling through all possible linear combinations of HH and VV (all filters). Each FIR filter on the x axis is applied to the image data to produce a solution image. An objective function is calculated for each solution image and the results plotted on the y axis. For the foreground (A), the objective function is the difference between samples of rough and smooth areas chosen from the solution images; for the background (B), the objective function is the variance within the samples of rough and smooth areas. The foreground/background surface is shown in (C).

(all combinations of C-band copolarized channels) and by calculating the objective function, we constructed a solution profile. Because all pixels are a mixture of foreground and background, it is also of interest to look at the profile that is formed by the ratio of the foreground to background (Fig. 5c). When we examine the profiles shown in Figure 5, our objective for an individual image might be to choose solutions that maximize the foreground/background contrast or solutions that simply minimize the background effects (see next section) to reduce contamination of the solution. However, in comparing profiles for two data takes, we see that there is a trough in the solution profiles where not only is the background reduced, but the solutions for DT 35.01 and DT 120.30 become similar (less look-direction dependent).

In Figure 6, the foregoing analysis is extended to include both C- and L-band copolarized channels. Here we produce solution surfaces, rather than profiles, where the x and y axes are now the C-band and L-band weights. Each axis again contains two variables (the w values for HH and VV). The x-y plane contains all possible ratios of HH and VV polarizations for C- and L-band. Each linear FIR filter in the x-y plane is applied to the images, and the objective functions are calculated to construct the solution surfaces. The resulting solution surfaces for DT 35.01 (Fig. 6) are characterized by a large plane where solutions have similar foreground/background ratios and by a localized trough. The SEM, IEM, and empirical FBA solutions are examples of solutions that lie in the plane.

Example solutions from the trough region are shown in Figure 7. Figures 7a and 7b show results obtained

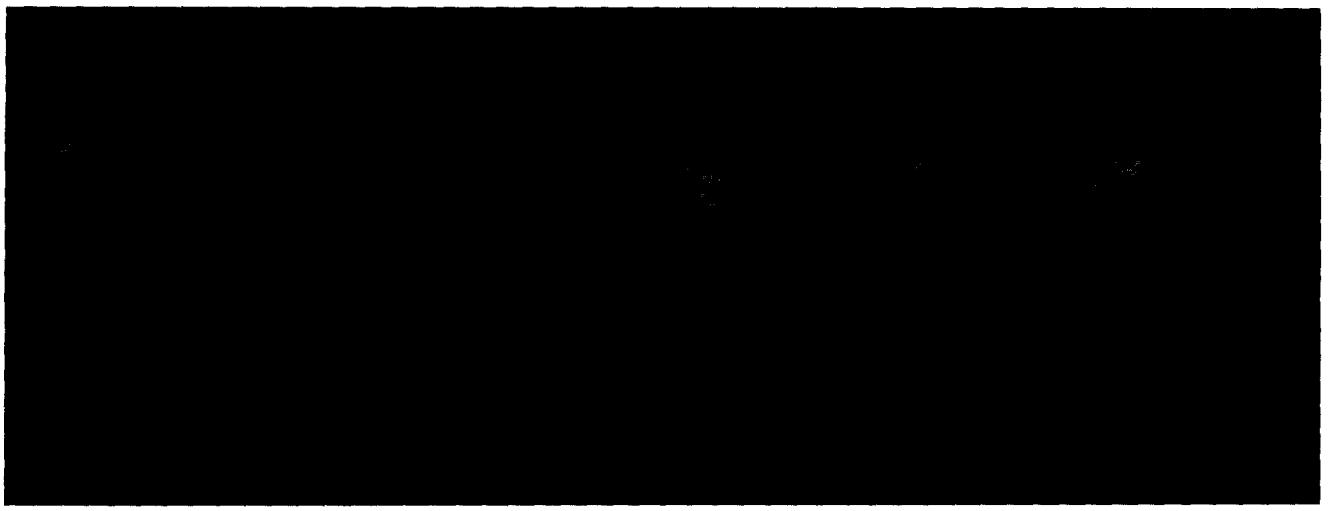

Figure 6. Surfaces generated from FIR filters designed to estimate rms height. Each 36×36 surface is formed by generating FIR filter weight (e.g., w_n vector) at 5° intervals over a range of 0° to 180°. The w_n vector element corresponding to the HH SAR measure is the sine of the angle, and that corresponding to VV is the cosine of the angle for both C- and L-bands. The x axis corresponds to C-band and the y axis to L-band. (A) Foreground contrast, the absolute value of the mean difference in roughness between image data points from the fans below Kit Fox Hills and the Grotto Canyon Fan. (B) Background, weighted average of the separate standard deviations of the pixels defining the foreground and background. (C) The foreground divided by the background.

from L-band copolarized channels for SIR-C DT 35.01 and AIRSAR data take CM 3588 (using the same FIR filter). These images also have contrasting look directions (see Table 2). Figures 7c and 7d show results from C- and L-band copolarized channels for DT 35.01 and DT 120.30 (again using the same FIR filter for each).

DISCUSSION

Empirical FBA, SEM, and IEM Results

Many of the differences observed between the FBA, SEM, IEM encountered in the preceding section are probably a consequence of the fact that the SEM and IEM inversion algorithms were developed and tested on a specific surface type—agricultural soil surfaces. Potential differences between agricultural soil surfaces and geological surfaces are many, but here we focus on two areas of contrast: the distribution of roughness with scale (in particular, the presence of intermediate-scale roughness) and the detailed geometry of the intrinsic surface roughness itself.

In contrast with agricultural fields, there are multiple scales of roughness in Death Valley, and they clearly pose a problem. The washes that descend the alluvial fan surfaces give rise to topography on the scale of meters to several meters (intermediate-scale roughness). Because inversions for surface roughness from SAR data are focused on roughness at the radar-wavelength scale (intrinsic roughness), the presence of intermediate-scale roughness probably helps explain the SEM and IEM overestimation of rms height (Fig. 3). In addition, this topography has a preferred azimuthal orientation controlled by the slope of the alluvial fans. The look direction of DT 35.01 is primarily at right angles to the mean wash orientation, whereas that of DT 120.30 is primarily parallel to the mean wash orientation. This suggests that intermediate-scale topography may account for the look-direction differences illustrated in Figure 4.

Another potential contrast with agricultural surfaces lies in the detailed geometry of intrinsic surface roughness. Because a complete mathematical description of the surface geometry (intrinsic roughness) may require as many as five parameters (Goff, 1995), it is possible for very different types of surface to have the same rms height and yet yield a very different backscatter. As we show here, even the surface power spectrum offset and slope, which represent a more complete description than rms height, do not adequately define surface type. In Figure 8, we illustrate two-dimensinal scattering calculations of radar backscatter (Pak et al., 1996; Tsang et al., 1994) for three different types of microtopographic profiles. The solid line in Figures 8a and 8b shows the scattering coefficient for real topographic profiles from one of the sites in Death Valley, and the dotted line shows the coefficient calculated for simulated profiles having the same average spectral slope, offset, and rms height as the real profiles. The profiles are Monte Carlo simulations made by taking the inverse Fast Fourier Transform (FFT) of the power-law fit to the mean power spectrum determined from the real profiles and by assuming random phase. The dashed line shows the calculated backscatter for simulated profiles again generated by using the power-law fit to the mean surface spectrum but with the nonrandom phases determined from the real profiles

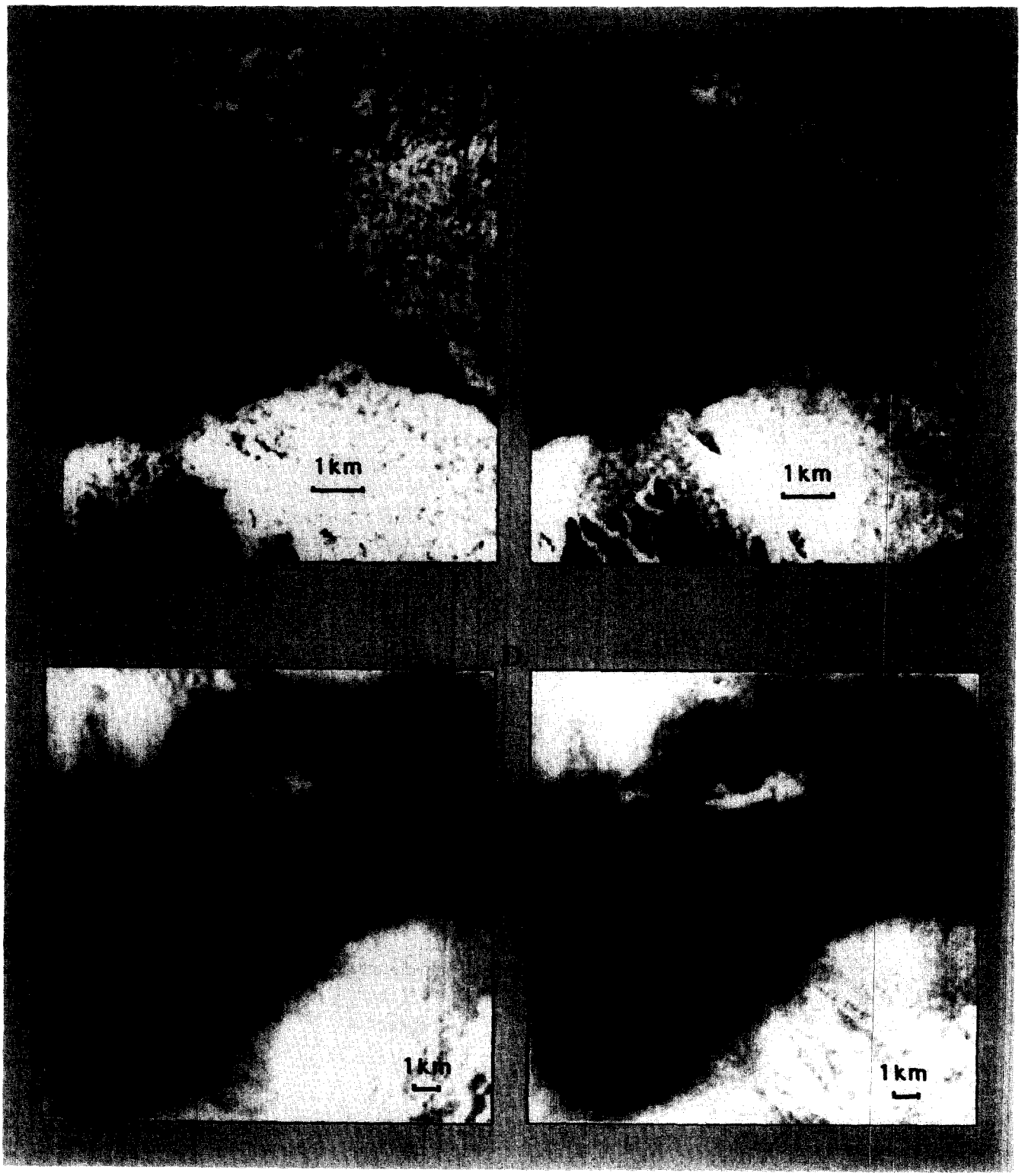

Figure 7. Example of the type of solution that occurs within the trough of the foreground/background profiles and surfaces (Figs. 5 and 6). Such a solution appears to minimize the local variance. In (A) and (B), the foreground is designated by the roughest areas of the image and the background by the smoothest areas in the image. (A) Application to AIRSAR data, using L-band copolarized channels. (B) Application to SIR-C data take 35.01 [same FIR filter as in (A)], using L-band copolarized channels. (C) Application to SIR-C DT 35.01, using L- and C-band copolarized channels. (D) Application to SIR-C DT 120.30, using L- and C-band copolarized channels.

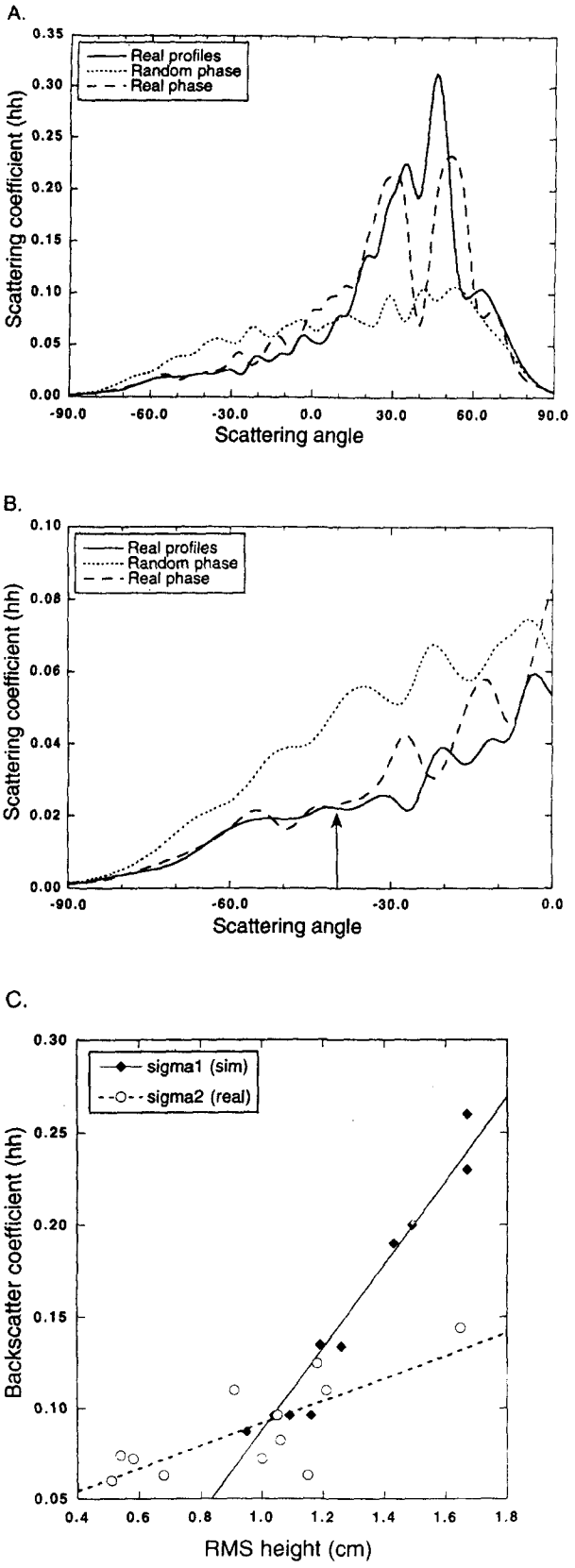

Figure 8. Results of forward modeling of radar scattering, using exact two-dimensional solutions (Tsang et al., 1994). (A) Scattering coefficient with scattering angle for three different types of surface profile (length approximately 1 m): the solid line shows averaged results from 40 real profiles at a site above the Kit Fox Hills in Death Valley; the dotted line shows results from profiles simulated by using the best-fit power law to the mean spectrum of the real profiles together with random phase; and the dashed line shows results for profiles also simulated by using the power law but combined with the real phases taken from spectra of the 40 real profiles. (B) An expansion of the backscatter part of (A). The arrow indicates the monostatic backscatter value (−40°). (C) The calculated backscatter coefficient against rms height for each of the sites in Death Valley together with linear best fits: solid symbols and solid line show the results for profiles simulated as in (A, dotted line); open symbols and dashed line show results for the real profiles (20 per site).

added to these best-fit spectra. The random-phase simulated profiles are unlike the real profiles in appearance; the roughness is much more distributed in the simulated surfaces. The organization of the real surface into discrete objects (pebbles) is reflected in the phase of the surface FFT, which is nonrandom. The calculated backscatter from the two types of surface is very different, with the simulated profiles having a much greater backscatter for the rougher surfaces. In this case, nonrandom phase seems to allow much more forward scatter and, correspondingly, there is less backscatter. However, the random-phase surfaces have a stronger rms-height dependence that results in overestimation of the real surface backscatter at the rougher end of the scale (greater than about 1 cm rms height for C-band) and underestimation of the backscatter for the smoother surfaces (Fig. 8c).

The phase of the surface power spectrum, therefore, plays a key role in determining the radar backscatter due to intrinsic surface roughness. Phase is a notoriously difficult quantity to analyze and, beyond the difference between random and nonrandom phase, we do not understand what characteristics of phase are important. A much more complete analysis would be required before its effects could be understood and predicted.

Generalized FBA Results

In FBA, effects on the SAR backscatter of the intermediate-scale roughness and the phase aspect of surfaces would be labeled as background effects that can propagate into the solution for the foreground (surface rms height). The generalized FBA approach was developed in response to these issues.

Generalized FBA reveals a large domain of solutions that are very dependent on the values of the input parameters. Empirical roughness estimates determined by using the field roughness data, SEM, and IEM all fall into this category (see Fig. 6). However, the generalized FBA illustrated in Figures 5 and 6 also reveals a localized trough region of the solution space where solutions have a unique character and where the variability be-

tween solutions from DT 35.01 and DT 120.30 is much reduced (see Figs. 5 and 7). In this trough region, the effects of background factors (as we have defined them) are minimized, but this is also at the expense of foreground resolution, which also has a minimum in this region (but slightly offset). Because these solutions minimize variance within fan units of uniform roughness, they are spatially smooth solutions that resolve only three or four distinct levels of roughness. Broad fan units are clearly defined and coherent. Apparent lateral roughness variation along the fans emanating from the Kit Fox Hills (seen in the SEM and the IEM) is somewhat suppressed (especially when only one SAR frequency is used). About four levels of roughness are distinguished in going from the playa (rms height less than 0.5 cm) to the roughest areas of Grotto Canyon Fan (rms height greater than 1.2 cm).

The use of FIR filters to examine the entire set of linear solutions to roughness in Death Valley has, therefore, uncovered some surprising new solutions that display a more robust character than do existing algorithms and empirical solutions. The method is, however, dependent on the definition of the objective functions for foreground and background, and this is an area for future exploration. The objective function chosen in the foregoing FBA to represent the foreground is imperfect. The foreground was defined as the difference between surfaces of different roughness. Defined in this way, the foreground is still to some degree open to the influence of intermediate-scale topography and to phase effects, to name just two background factors. Hence it may be that minimization of background factors (rather than maximizing foreground/background contrast) presents the more robust route to a solution for roughness.

General Discussion

In general, the inversion of SAR data for surface roughness is extremely dependent on the complexity of the surface in question. In the case of flat-lying, bare soil surfaces it is perhaps possible that consistent and accurate results be obtained with existing methods (e.g., SEM and IEM). However, in the extension to more complex surfaces or surfaces of different character, the effects of background complexity will propagate into the solution for roughness in a generally unpredictable way. Note that it is the nature of the dependence between backscatter and roughness at the wavelength scale that appears to vary. Despite the complexity of the Death Valley alluvial fan surfaces, there is still a strong dependence of radar backscatter on surface roughness at the wavelength scale, but the dependency is different from that found for soil surfaces (Dubois et al., 1995). As a result, one can have a fairly high degree of success in producing a relative ranking of Death Valley surfaces by roughness, using the L-band amplitude, for example (Blumberg et al, personal communication), although in detail there will be errors. This strong relation between roughness parameters, such as power-spectrum offset and backscatter, suggests the possibility of retrieval of numerical roughness with a high degree of resolution. However, this is illusory unless we know beforehand the specific roughness-backscatter relation for the surfaces in question. If this is unknown, then numerical resolution of roughness must be sacrificed for robustness. The extraction of high-resolution numerical roughness would, therefore, rely on identification of surface type, and this might require the use of additional information other than the SAR data. Certainly, it would require all bands of SIR-C/XSAR data to minimize propagation of background into roughness determinations.

The motivation for this study was to develop solutions for intrinsic roughness that are extendible over a range of conditions. The degree to which our methods are extendible remains, however, to be verified and is the focus of continuing work.

CONCLUSIONS

In Death Valley, the radar backscatter is strongly related to the offset of the surface power spectrum and weakly related to the rms height. Inversions for these parameters are, however, affected by intermediate-scale roughness and by the phase character of the surface. The relation between roughness parameters and backscatter is thus a function of surface type.

Examination of the solution space, using FBA, shows that SEM, IEM, and empirical FIR (field-measurement driven) represent similar types of solutions that are very dependent on the values of the input image parameters—they are sensitive to the background variability. A smaller class of FIR filters was found that are more stable in this respect, but this stability is at the expense of reduced resolution of roughness. Only three to four roughness levels are resolved in Death Valley. There is a trade-off between resolution and consistency that appears to be intrinsic to this inverse problem. Hence, reduced resolution in solutions that are robust and extendible is unavoidable unless new data can be brought to bear on the inversion.

This work was supported by NASA/JPL Contract No. 958450. We thank J. C. Shi at the University of California at Santa Barbara for supplying results of the IEM model. We also thank four anonymous reviewers for their helpful comments and suggestions.

REFERENCES

Dubois, P. C., van Zyl, J. J., and Engman, T. (1995), Measuring soil moisture with imaging radars. *IEEE Trans. Geosci. Remote Sens.* 33(4):915–926.

Evans, D. L., Farr, T. G., and van Zyl, J. J. (1992), Estimates of surface roughness derived from synthetic aperture radar (SAR) data. *IEEE Trans. Geosci. Remote Sens.* 30(2): 382–389.

Farr, T. G. (1992), Microtopographic evolution of lava flows at Cima Volcanic Field, Mojave Desert, California. *J. Geophys. Res.* 97(B11):15,171–15,179.

Farr, T. G., Wall, S. D., Muller, J.-P., Lewis, P., and Lerberl, F. W. (1991), Measurement of surface microtopography. *Photogramm. Eng. Remote. Sens.* 57(8):1075–1078.

Farrand, W. H., and Harsanyi, J. C. (1996), Mapping the distribution of mine tailings in the Coeur d'Alene River Valley, Idaho, through the use of constrained energy minimization technique. *Remote Sens. Environ.* in press.

Goff, J. A. (1995), Quantitative analysis of sea ice draft, 1: methods for stochastic modeling. *J. Geophys. Res.* 100: 6993–7004.

Harsanyi, J. C. (1993), Detection and classification of subpixel spectral signatures in hyperspectral image sequences, Ph.D. Dissertation, Univ. Maryland, Baltimore, MD. 116 pp.

Oh, Y., Sarabandi, K., and Ulaby, F. T. (1992), An empirical model and an inversion technique for radar scattering from bare soil surfaces. *IEEE Trans. Geosci. Remote Sens.* 30(2): 370–381.

Pak, K., Tsang, L., Chan, C. H., and Johnson, J. T. (1995), Backscattering enhancement of vector electromagnetic waves from two-dimensional random rough surfaces based on Monte Carlo simulations. *J. Opt. Soc. Am. A* 12(11): 2491–2499.

Shi, J. C., Wang, J., Hsu, A., O'Neill, P., and Engman, E. T. Estimation of bare soil moisture and surface roughness parameters using L-band SAR image data. *IEEE Trans. Geosci. Remote Sens.* IGARSS'95 special issue, in press.

Smith, M. O., Roberts, D. A., Hill, J., Mehl, W., Hosgood, B., Verdebout, J., Schmuck, G., Koechler, C., and Adams, J. B. (1994), A new approach to determining spectral abundances of mixtures in multispectral images. *IEEE Trans. Geosci. Remote Sens.* Proc. IGARSS'94, JPL, Pasadena, CA.

Smith, M. O., Weeks, R. J., and Gillespie, A. R. (1996), A strategy to quantify moisture and roughness from SAR images using finite impulse response filters. *IEEE Trans. Geosci. Remote Sens.* Special issue on retrieval of geo- and bio-geophysical parameters, submitted.

Tsang, L., Chan, C. H., and Pak, K. (1994), Backscattering enhancement of a two-dimensional random rough surface (three-dimensional scattering) based on Monte Carlo simulations. *J. Opt. Soc. Am.* 11:711–715.

van Zyl, J. J., Burnette, C. F., and Farr, T. G. (1991), Inference of surface power spectra from inversion of multifrequency polarimetric radar data. *Geophys. Res. Lett.* 18(9):1787–1790.

Weeks, R. J., Smith, M. O., Pak, K., Li, W.-H., Gillespie, A. R., and Gustafson, B. (1996), Surface roughness, radar backscatter and VNIR reflectance in Death Valley, California, *J. Geophys. Res. Planets.* 101(E10):23,077–23,090.